Hindawi
Geofluids
Volume 2023, Article ID 9255499, 11 pages
https://doi.org/10.1155/2023/9255499

Research Article

Fractured Zone Detection Using Petrophysical Logs by Rescaled Windowed R/S Analyses and Discrete Fracture Network (DFN) of Yanchang Formation in Mahuangshan-Hongliugou Area, Ordos Basin, China

Jindong Gao,[1,2] **Lirong Li**,[2] **Gaorun Gao**,[3] **Shuwei Ma**,[4] **and Meng Li**[5]

[1]*Key Laboratory for Digital Land and Resources of Jiangxi Province, East China University of Technology, Nanchang 330013, China*
[2]*School of Earth Sciences, East China University of Technology, Nanchang, China*
[3]*School of Petroleum Engineering and Environmental Engineering, Yan'an University, Yan'an, Shaanxi 716000, China*
[4]*Research Institute of Exploration and Development, PetroChina Changqing Oilfield Company, Xi'an, Shaanxi, China 710018*
[5]*China Railway First Survey and Design Institute Group Ltd., Xi'an, Shaanxi 710043, China*

Correspondence should be addressed to Jindong Gao; 13396251993@163.com

Received 1 December 2022; Revised 1 September 2023; Accepted 11 September 2023; Published 28 September 2023

Academic Editor: Mohammed Fattah

Structural fractures generally develop in the upper crust strata and are usually distributed in a convergent pattern, forming structural fracture zones with a specific strike. Fracture zones control the reservoir seepage system and seriously affect the migration and accumulation of oil and gas in tight sandstone reservoirs. Therefore, characterizing the characteristics of the fracture zones for tight oil exploration and development effectively is essential. In this paper, the variable scale fractal method is introduced to calculate the petrophysical log, and a new curve H is built. An intensity log is to characterize the intensity of structural fracture development. The H curve is in a good linear relationship with the intensity curve after the comparison of the H curve and intensity curve in 32 wells. A quantitative relationship between H and the intensity curve is established. Based on the parameters obtained from the core and image logs, the discrete fracture network model was established using H curves from more than 300 wells, and the structural fracture zone was analyzed. The model shows that the fracture zones formed by structural fractures are in S-N and NW-SE directions in the study area. The orientation of the structural fracture zone is consistent with that of the fractured fault zone and fault, and the development of the fractured zone is consistent with the regional tectonic evolution characteristics. The characteristics of the fracture zone explain the distribution law of oil accumulation and groundwater salinity in the study area.

1. Introduction

Fractures, on a large or small scale, are commonly seen within the earth's crust and form complex discrete fracture networks (DFN) [1, 2]. The complex DFN made up of fracture zones transfers a concentration of fractures into a narrow tabular zone, in which the structural fractures are at stable attitude [3–7]. Fractures control hydrocarbon accumulation, and oil and gas reservoirs are easy to develop in the dominant strike direction of fracture zones. This phenomenon is more prominent in tight sandstone reservoirs [8–11]. Therefore, understanding the spatial distribution of fracture zones is essential to the effective exploration and rational development of tight sandstone oil and gas resources [8, 12, 13].

Fractures can probably be detected directly or indirectly using outcrop or core description, petrophysical logs, seismic interpretation, etc. [14–16]. However, these data are usually collected from lower dimensional limited exposures, e.g., borehole logging (one-dimensional (1D)) and outcrop mapping (two-dimensional (2D)). Seismological data is not effective when detecting medium and small fractures due

to its resolution [17, 18]. Therefore, a complete measurement of a 3D fracture system is difficult, and the description of fractured zones has to largely rely on extrapolations, which use statistics from 1D/2D to 3D and from small samples to the whole study area. The stochastic DFN modeling uses an object-oriented geostatistical modeling method to construct the overall fracture system according to the occurrence, location, and interrelationship of various fracture groups in a 3D space, and the method provides a reasonable network for finite-sized fracture population evaluation in unknown areas [19, 20].

As small samples usually lead to misleading interpretations in the modeling, any direct or indirect data increasing the understanding of fracture properties is highly valuable. In the borehole, the structural fracture network is crosscut by the "line" (the well itself), forming a point sequence. Petrophysical logs are commonly available, and they help to collect the response from fractures. Therefore, it is vital to know how to use petrophysical logs to detect fractures and predict fracture distribution. Most of the previous studies were either too theoretical or too data processing. They suggested that any single petrophysical logs could not unequivocally indicate the presence of fractures [21, 22]. More data processing methods were proposed to extract more information from petrophysical logs, such as wavelet transform and wavelet decomposition [23–25], factor analysis [26], regressions analysis [27], and deep learning and neural networks [28]. However, most of the methods were developed for several limited wells or specific geological conditions, and the previous studies were either inadequate in data or lacked validation [29]. Thus, it is difficult to generalize and generate the DFN model with those methods [30]. In recent decades, fractal geometry has been applied in the analysis of geological phenomena and geophysical data processing [31–35]. For example, the linear density of fractures (P10) can be characterized by the calculation of the fractal dimension of geophysical logging data, and the variable bandwidth R/S method was introduced to evaluate the linear density of fractures [36–38].

In this paper, we take the Upper Triassic Yanchang Formation of the Jiyuan area in Ordos Basin, China, as an example. A fractal geometry method-rescaled windowed R/S analysis is presented to estimate fractured zones with petrophysical logs (acoustic logging and natural gamma ray spectral log), simple linear estimators established between the results of the proposed methodology, and the intensity logs obtained from image logs. More than 300 vertical wells were analyzed by this methodology, and the results were applied to a geostatistically derived density field to build DFN. A large volume of data has been applied, which enables us not only to check the accuracy of the method but also to study the possibility of its generalization [27, 39].

2. Geology Setting

Ordos Basin is multiple superimposed basins of Paleozoic and Mesozoic and is an east-to-west dip monocline with and dip angle of less than 1° [40]. Structural fractures are popular in Mesozoic of the basin, with stable attitude and convergent distribution. The structural fractures on the outcrop consist of a wide range and regular development of structural fractured zones and constitute a good fracture network system [5]. According to 24 image logs and 627.6 m core observations from 42 wells, the structural fractures in the Jiyuan area are mainly distributed in tight sandstone formations with four dominant strike directions: NEE-SWW, NW-SE, NNW-SSE, and NE-SW. NEE-SWW and NW-SE and NNW-SSE and NE-SW constitute two groups of conjugate shear fractures, in which the conjugate shear fractures in NEE-SWW and NW-SE orientation are dominant (Figure 1(a)) [41–44]. The dip angle of fractures is mainly distributed between 80° and 90°, and the proportions of high angle (>75°), oblique angle (45°~75°), and low angle (<45°) fractures were 73.7%, 14.6%, and 11.7%, respectively. Fractures are mainly controlled by rock strata, and the height of fractures in the borehole of 0.05~2.5 m accounts for 97%. The fracture opening is mainly concentrated in 0~1 mm, while more than 70% of the fractures are not filled by other minerals, and most of the rest are half-filled or partially filled, still retaining part of the void [45].

The study area is located in the Mahuangshan-Hongjingzi-Hongliugou-Fengdigou area in the northwest of the Jiyuan region. Faults in the northern part of the study area, presenting an NE-SW strike direction, gradually weakened from the northwest to the study area. In the study area, faults are void, and nose structures are generally developed (Figure 1(b)). The modeling area contains more than 300 petrophysical logs and three image logs. By comparing H curves from 24 wells in the Jiyuan area with intensity logs, which identify fracture zones and the number of fractures in each fracture zone (fracture density), we obtained fracture density estimating for fracture zones that can be generalized to all wells. Calculations from more than 300 conventional logs were used to analyze the distribution characteristics of tectonic fractures in the DFN region.

3. Methods

DFN modeling contains two consecutive steps. First, the geometric parameters of the individual fractures must be determined. These parameters are the foundation for the modeling [48]. The most important geometric parameters are the fracture length distribution, the attitude of the fractures, their aperture, and the spatial density of fracture midpoints. The first three parameters can be obtained from core and image logs, and the variable bandwidth R/S method was introduced to evaluate the linear density of fractures while image logs are not valuable. Second, the network is generated using a fracture modeling software program. In this study, we use Petrel to build discrete fracture network modeling [48, 49].

3.1. The Variable Bandwidth R/S Method. The R/S method defines the ratio of the maximum cumulative deviation R (the value defined in (1)) to the standard deviation S (the value defined in (2)) of a time series as the relative fluctuation intensity of the time series; the Hurst index is determined by linear regression of all possible sets of values of

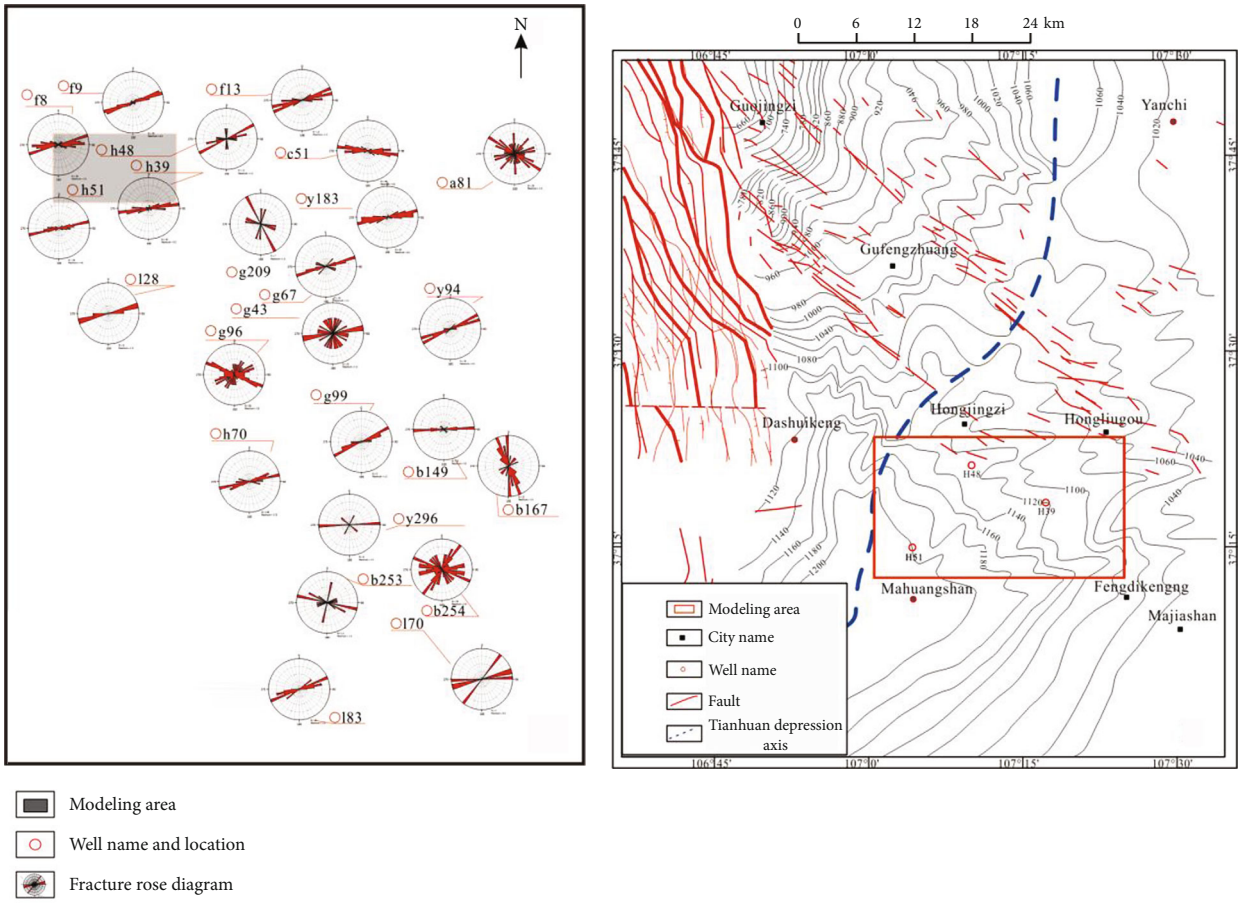

FIGURE 1: (a) Logging interpretation results and modeling area location of Triassic Yanchang Formation in Jiyuan area. (b) Location and surrounding structural characteristics of modeling area (according to [46, 47]).

log (n) against log (R/S) (the value defined in (3)) [50]. The Hurst index represents the drastic change in reservoir discharge, and it can quantitatively evaluate the complexity of one-dimensional time series simply and effectively. Petrophysical log curves of oil wells are fixed in sampling frequencies and self-similar fractal characteristics, so they can be regarded as one-dimensional time series, and the roughnesses of the curves can be measured via the R/S method. It is found that too many or too few log (R/S) and log (n) data sets in the R/S method are not able to effectively mine the nonlinear and discrete characteristics of structural fractures [48, 51]. In addition, if the calculation interval is not constrained, the back data will participate in the calculation in each calculation process, resulting in an excessive repetition of the calculation process. Meanwhile, the calculation result of the rear data will affect the calculation result of the H index.

$$R(n) = \max_{o<u<n}\left\{\sum_{i=1}^{u} Z(i) - \frac{u}{n}\sum_{i=1}^{u} Z(j)\right\} - \min_{o<u<n}\left\{\sum_{i=1}^{u} Z(i) - \frac{u}{n}\sum_{i=1}^{u} Z(j)\right\}, \tag{1}$$

$$S(n) = \sqrt{\frac{1}{n}\sum_{i=1}^{u} Z^2(i) - \left[\frac{1}{n}\sum_{i=1}^{u} Z(i)^2\right]}, \tag{2}$$

where Z is the time series where R/S analysis needs to be performed, n is the total number of log data sampling points, u is a sample point that begins to increase between 0 and n, and i and j represent the variables of the number of sample points [52, 53].

$$\mathrm{R/S} = \frac{R(n)}{S(n)}. \tag{3}$$

Using the variable bandwidth R/S method, firstly, the profile of length L is divided into windows or "bands" of width m, and the H value of the band is calculated. The middle point depth (t) is taken as the depth of the H value of the band. $R(t, n, m)$ is the R/S value of the petrophysical log within a scaled window m, t is the depth of the scaled window, n is the point number of one step (or the step length), and m is the point number petrophysical signals within scaled window. Then, the H value of the next band is calculated by using n as a step size. The H values of each band are

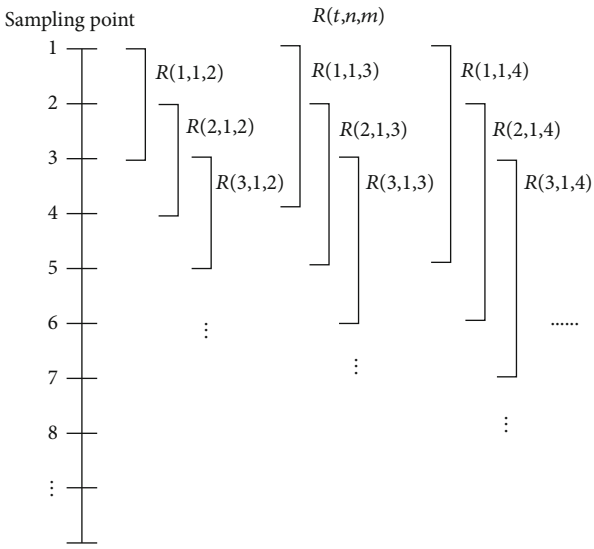

Figure 2: The schematic of the calculation of H by R/S analysis algorithm (modified according to [45]).

calculated in turn, and a series of H values with a specific depth form a one-dimensional series is called the H curve [52, 54]. The analysis algorithm is written in MATLAB (Figure 2).

3.2. Intensity Log and Petrophysical Log Energy. Borehole imaging logs define the exact spatial location of fractures, so the intersections between fracture networks and boreholes can be interpreted as point processes. Based on core and image log data, the validity of 24 calculated H curves indicating fractures was analyzed. To facilitate quantitative comparison, an intensity log (formula (4)) was introduced to evaluate the development degree of structural fractures.

$$\text{Intensity}\,(\text{MD}) = \frac{\text{cumulative}\,(\text{md} + w/2) - \text{cumulative}\,(\text{md} - w/2)}{W}. \tag{4}$$

where intensity (MD) is its value at the depth of md, cumulative $(\text{md} + w/2)$ is the cumulative fracture number at the depth of $(\text{md} + w/2)$, and W is the interval depth (m^{-1}).

Evaluation of fracture development intensity log and H curve is calculated by curve energy (E_H) parameter (formula (5)).

$$E_H = \sum_{i=1}^{n} H_i^2, \tag{5}$$

where H and n are the value of the H curve and the number of H curves in each fractured zone, respectively [27].

3.3. The Choice of Petrophysical Logs. The heterogeneity in the downhole is usually caused by lithologic changes and reservoir petrophysical heterogeneity. To identify fractures by conventional logs, it is necessary to enhance fracture responses and eliminate nonfracture influence [55]. Porous medium models and porous medium elastic wave theories have been developed to use acoustic data to detect fractures because the presence of fractures leads to anomalies in acoustic waves [56, 57].

Table 1: Calculation parameters of band length and step length.

	Band length (m)	n length (m)
The data mount	10	10
	10	5
	10	2.5
	5	5
	5	2.5

Sonic log (DT) measures a formation's interval transit time, while pore and fracture in a formation affect the interval transit time in many aspects. So DT not only reflects the vertical heterogeneity caused by lithological changes but also pores and fractures. Therefore, H of the DT log shows vertical heterogeneity characteristics of local petrophysical changes superimposed based on lithological changes. H of GR reflects the vertical heterogeneity caused by lithologic cycles. Thus, the difference between H of DT logs and that of GR logs may represent the heterogeneity caused by fractures [58, 59]. H curves are the difference between the DT and GR Hurst index.

4. Results

First, the petrophysical logs corresponding to the image logs of 24 wells in the Jiyuan area were standardized. According to the height of structural fractures in image logs, the bandwidths (m) were 5 m and 10 m, and the step sizes (n) were 2.5 m, 5 m, and 10 m. The R/S method with variable bandwidth was used to calculate H curves from 24 wells based on the parameter combinations in Table 1 [45].

Results calculated using different parameter combinations show that the positive amplitude of ~2382, ~2430, ~2475, ~2500, ~2515, ~2555, and ~2575 in well G96 is obvious. The corresponding image logs show that the fracture zones are developed at ~2380, ~2425, ~2470, ~2520, ~2545, ~2582, and ~2620 m. Core observation results show that 2345~2360, 2380~2390, 2410~2428, 2450~2455, 2460~2475, 2505~2545, 2505~2595, and 2615~2630 are segments during which fracture develops (Figure 3). In well A81, ~2060, ~2086, ~2120, ~2152, and ~2166 show an obvious positive amplitude, and the corresponding image logs show that ~2086, ~2110, ~2126, ~2150, and ~2170 m are fracture zones. Core observation results show that 2050~2094, 2108~2120, 2130~2150, 2166~2176, and 2186~2194 are fracture development sections (Figure 4).

5. Discussion

5.1. Correlation between Energy Log and Fracture Density. Theoretically, the positive anomalous amplitude of the H curve indicates the structural fracture zone. Compared with the intensity logs interpreted by image logs, the H curve

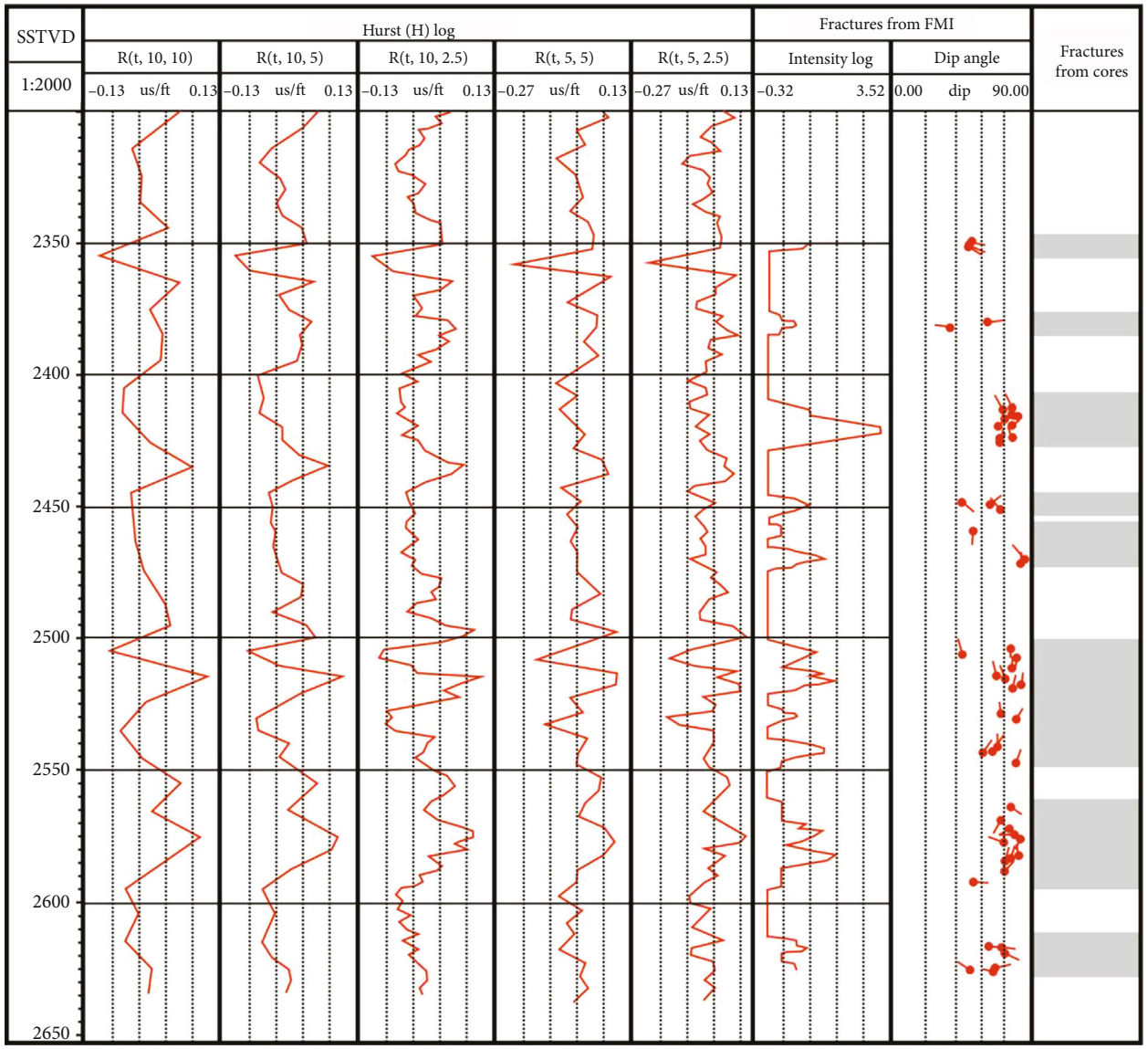

Figure 3: Comparison of intensity log and H curves of well G96.

calculated by the variable bandwidth R/S method with different parameter combinations is different in resolutions when applied in structural fracture zones. For example, in well A81 ranging from 2015 to 2019 m, the H curve calculated by (10, 10) shows only one peak and cannot distinguish between two fracture zones. Although (5, 2.5) can distinguish two fracture zones, there are multiple peak values, easily leading to wrong interpretation. (10, 2.5) reasonably constrains the structural fracture zone, and the H curve calculated by this combination is the best constraint effect on the structural fracture zone (Figures 3 and 4). However, because fractures are mainly at high angles, lateral detection depth (n cm) of DT logging is several times than that of FMI detection depth (~5.08 mm). Therefore, the fracture zone depth in the H curve may not correspond strictly to the intensity log depth, and a difference of ±5 m between them is reasonable.

The detection result of the energy curve of the H curve reached a 91.67% similarity with intensity logs and the result of cores (Figure 5). This method is accurate in estimating fracture density in the fracture zone. If the correlation between the energy curve of the H curve and the intensity log can be established, this method can be extended. Tokhmechi et al. [27] studied that the DT energy curve and fracture intensity logs had a nonlinear relationship (exponential type). Therefore, the energy curve (NH) of the H curve is positively correlated with fracture intensity logs (FD). The H energy curve and fracture development intensity curve of the whole well section were in linear regression:

$$\mathrm{FD} = a^{*}\mathrm{NH} + b. \tag{6}$$

Statistical analysis of the H energy curve and fracture development intensity curve in the whole well section of 24 wells shows that the prediction accuracy of the energy curve of the H curve is 73.3% (Figure 6).

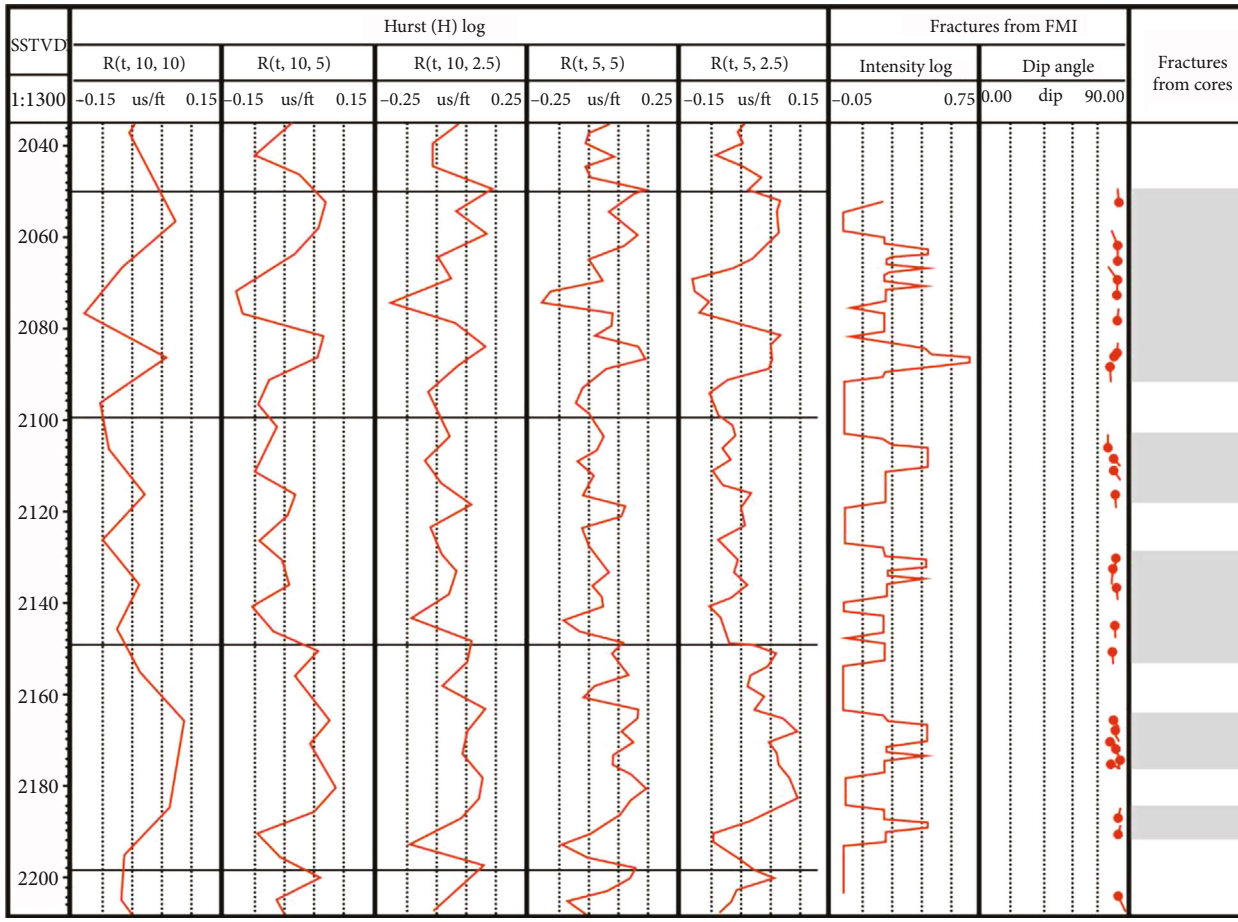

Figure 4: Comparison of intensity log and H curves of well A81.

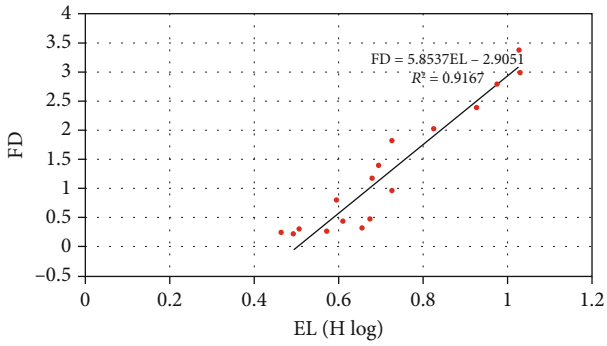

Figure 5: Linear regression between fracture zone energy log and fracture density.

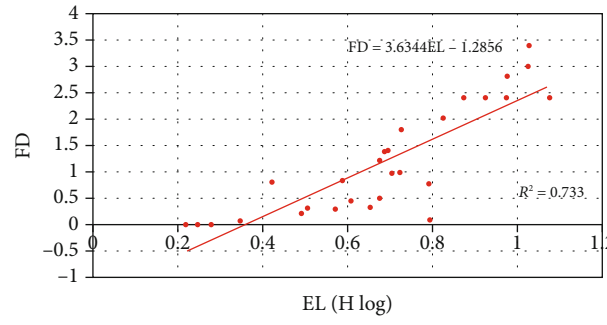

Figure 6: Linear regression between fracture zone energy logging and fracture density throughout the wellbore.

5.2. Fracture Network. The discrete fracture network modeling is applied by the software Petrel, and structural fractures were set as a planar quadrilateral in modeling; attitude, length, and breadth of structural fractures were obtained by the statistics of the image log and core observation data. There was a strong exponential relationship between the length and the height of structural fractures [12, 60]. Detailed parameters of structural fractures can be found in [45].

Constructing a DFN model in Petrel consists of the following steps:

(1) Data loading

The data used to create the 3D model consisted of ASCII files with coordinates in XYZ format describing the surfaces, 47 well logs' file containing$H$curves calculated by the variable bandwidth R/S method, and ASCII files with dip angel, dip azimuth, and coordinates in XYZ format describing the fractures obtained from imaging logging data.

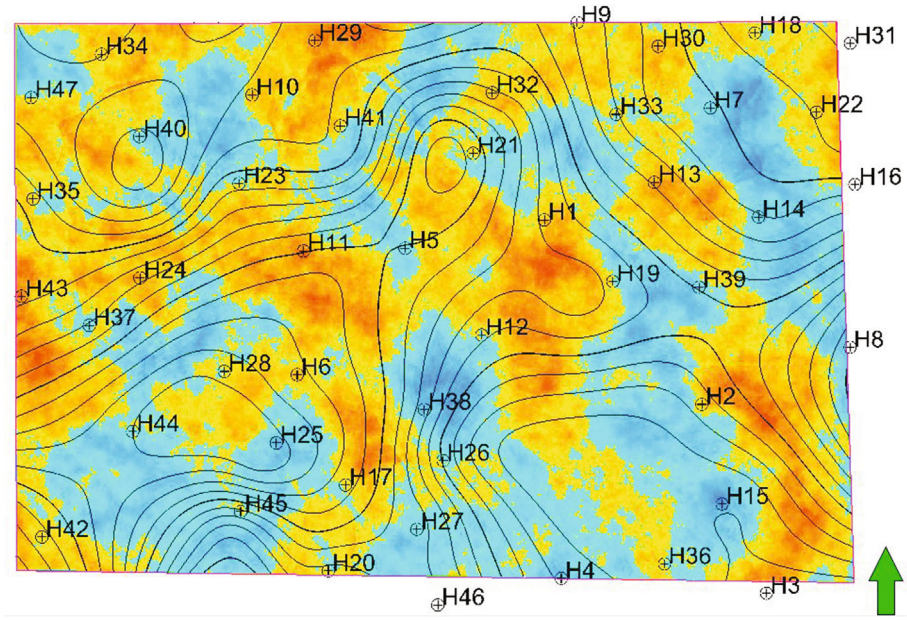

Figure 7: Fracture density model of the study area.

(2) Creation of surfaces

The first step in building a 3D model is to convert the XYZ points into surfaces. A convergent interpolation algorithm in the "Make/edit surface" process was used. The convergent interpolation algorithm is an iterative algorithm which converges on the solution (a final surface) by each iteration [61].

(3) Creation of horizons and zones

For the surfaces to be incorporated into the 3D grid, they needed to be transformed into horizons which was done in the "Make horizons" process [61].

(4) Upscaling

The H curves corrected with the proposed linear relationship were used to characterize the fracture density without FMI. The fracture intensity curve and tadpole map are generated with the imported fracture data. Then, upscaling was done to upscale the log data (intensity logs and H logs) to the cells. Each cell being penetrated by the well was given a single value of the property in question; the density of two-stage group fractures was assigned to the corresponding grids. After the cells being penetrated by the wells had been detected, the log data falling into the cells were averaged depending on which averaging algorithm that was chosen. The fracture density model of the study area was calculated by random modeling method (Figure 7).

(5) DFN simulation

The discrete fracture network is generated based on the fracture density attribute. The fracture units with certain spatial position, attitude, shape, and opening were randomly located, and the fracture system satisfies two-stage group characteristics (Figure 8).The fracture model is established deterministically based on the fracture sheet obtained by ant tracking. Generate fracture properties, such as fracture porosity and permeability.

The fracture density model shows that structural fractures in the modeling area form a wide and regular fracture zone in space (Figure 7). The structural fracture zone presents S-N and NW-SE directions, which is consistent with the strike direction of Guozhuangzi-Gufengzhuang-Hongliugou faults in the north (Figure 1).

The experimental process of rock mechanics shows that the fracture process is a development and evolution process of microfractures, and the formation of structural fractures and faults can be the material manifestation of different stages of the evolution during the same tectonic stress. The complex loading history and evolution of spatial heterogeneity in the rock result in a complex discrete fracture network (DFN) [1, 45]. Structural fractures in the study area are formed by horizontal tectonic stress. During late Yanshan movement with NW-SE extrusion stress inside the basin, the western margin of the basin is affected by the tectonic action and formed a large number of E-W and NW-SE to conjugate shear fractures in Gufengzhuang-Hongjingzi. They even develop into a small fault or structural fracture in the study area but with a smaller density. During the Himalayan movement, S-N and NE-SW conjugate shear fractures were formed under NE-SW regional stress compression, and the S-N structural fracture zone was formed in space. The earlier fractures were aggravated by the Himalayan tectonism, and the E-W and NW-SE conjugate shear fractures were further strengthened in the study area, forming faults in the area of Guozhuangzi-Gufengzhuang-Hongliugou. Two fracture zones with dominant strike directions were formed in the study area, forming a structural fracture system superimposed on each other (Figure 8). Development of structural fracture zones in the study area

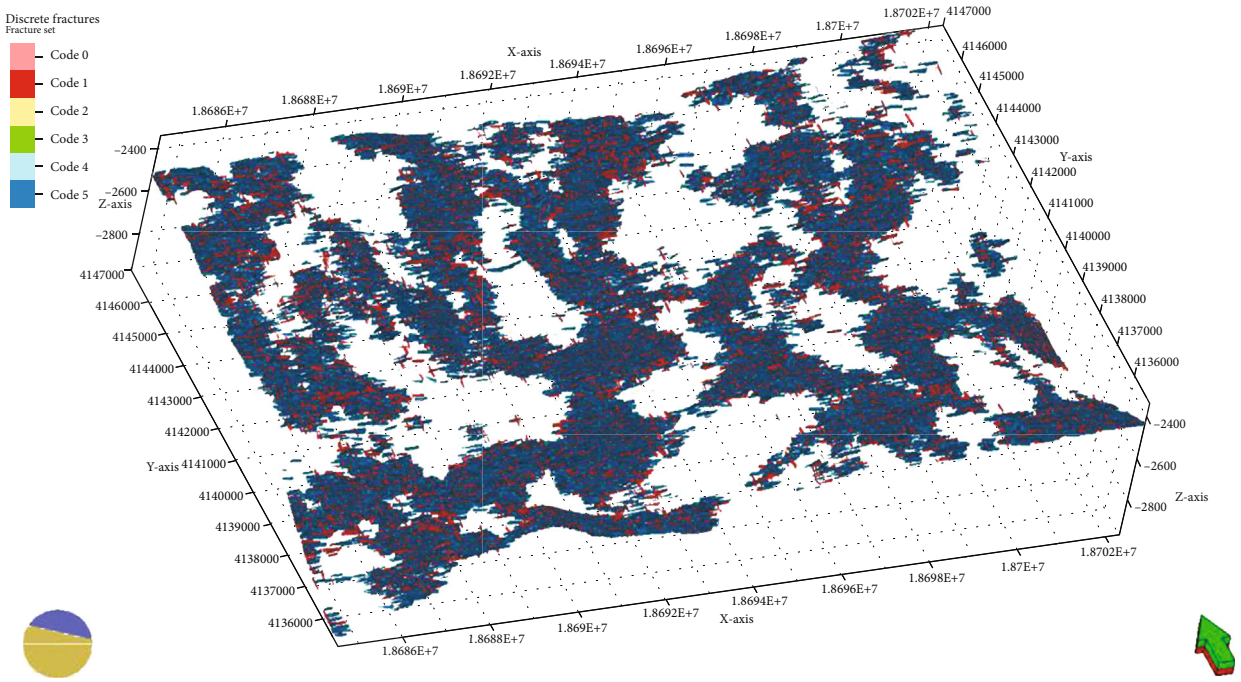

Figure 8: Discrete fracture network model.

plays a controlling role in the tight oil accumulation of Yanchang Formation. The fracture zone communicates shallow groundwater with oil accumulation, which significantly reduces the salinity of the formation water in the tight reservoir [62].

6. Conclusion

This paper proposes a variable bandwidth R/S method to estimate fracture density in fractured zones using petrophysical logs. 24 image logs and 627.6 m of cores from 42 wells in the study area were used to identify fractured zones and fracture density. To find a better-generalized estimator, 24 intensity logs were calculated with image logs, and the corresponding H curves of 24 petrophysical logs were calculated by the variable bandwidth R/S method as the base data. Linear regression is utilized between intensity logs and H curves. 47 H curves are applied to a geostatistically derived density field, and the DFN model was built. According to the results, the variable bandwidth R/S method is effective and propagable.

In conclusion, the findings of this paper are the following:

(1) The variable bandwidth R/S method is used to calculate the acoustic time difference log (DT) and natural gamma ray (GR) curves, and the H curves are established by the difference between the two curves. The comparison between the energy curve of the H curve and the intensity curve shows that the H curve is effective in predicting fracture density. Under the constraints of the results of core and image log interpretation, a simple linear relationship can be established between H curves and intensity log, FD = 5.8537*NH − 2.9051. After a linear operation, the fracture intensity represented by the H curve can be extrapolated to establish the fracture intensity model and constrain the establishment of the DFN model

(2) In the DFN model established by the fracture density model, the structural fractures are zonal, and the overall structure fractures are near S-N and NW-SE trending. Distribution characteristics of the structural fracture zone are consistent with the development characteristics of regional faults and fractures, verifying that the study area belongs to the weak structural deformation area

(3) The NW-SE trending structural fracture belt was formed during the Yanshanian tectonism, and the S-N trending structural fracture belt was formed during the Himalayan tectonism. NW-SE structural fractures were strengthened during Himalayan tectonism. The development of a structural fracture zone controls the distribution of the tight oil reservoir of the Yanchang Formation in the study area and results in a significant difference in the formation of water salinity in the tight oil reservoir

Data Availability

The data will not be made available due to commercial confidentiality.

Conflicts of Interest

The authors declare that they have no conflicts of interest.

Acknowledgments

The study is supported by the Science and Technology Research Project of Education Department of Jiangxi Province (GJJ2200757).

References

[1] R. Albert and A. L. Barabasi, "Statistical mechanics of complex networks," *Review of Modern Physics*, vol. 74, no. 1, pp. 47–97, 2002.

[2] B. M. Yousef and D. A. Angus, "When do fractured media become seismically anisotropic? Some implications on quantifying fracture properties," *Earth and Planetary Science Letters*, vol. 444, pp. 150–159, 2016.

[3] E. Bonnet, O. Bour, N. E. Odling et al., "Scaling of fracture systems in geological media," *Reviews of Geophysics*, vol. 39, no. 3, pp. 347–383, 2001.

[4] J. M. Questiaux, G. D. Couples, and N. Ruby, "Fractured reservoirs with fracture corridors," *Geophysical Prospecting*, vol. 58, no. 2, pp. 279–295, 2010.

[5] L. B. Zeng, C. Y. Gao, J. F. Qi, Y. K. Wang, L. Li, and X. F. Qu, "Distribution and permeable of reservoir fractures, Longdong area of South Ordos basin," *Science in China: Series D, Earth Sciences*, vol. 38, Supplement, pp. 44–50, 2008.

[6] D. F. He, H. P. Bao, B. Z. Kai et al., "Critical tectonic modification periods and its geologic features of Ordos basin and adjacent area," *Acta Petrolei Sinica*, vol. 42, no. 10, p. 15, 2021.

[7] G. Hou and W. Pan, *Fracture Geological Modeling and Mechanical Mechanism*, Science Press, Beijing, China, 2013.

[8] T. Engelder, G. G. Lash, and R. Uzcátegui, "Joint sets that enhance production from Middle and Upper Devonian gas shales of the Appalachian basin," *AAPG Bulletin*, vol. 93, no. 7, pp. 857–889, 2009.

[9] J. H. Fu, S. X. Li, X. Y. Liu, S. Y. Yang, and A. X. Luo, "Multilayer composite accumulation mechanism and exploration significance of Jiyuan oilfield, Ordos basin," *China Petroleum Exploration*, vol. 18, no. 5, pp. 1–9, 2013.

[10] X. R. Luo, L. K. Zhang, Y. H. Lei, C. Z. Hu, H. Shi, and B. F. Cao, "Structural heterogeneity of reservoirs and its implication on hydrocarbon accumulation in deep zones," *China Petroleum Exploration*, vol. 21, no. 1, pp. 28–36, 2016.

[11] W. Z. Zhao, R. Zhu, S. Hu, L. Hou, and S. Wu, "Accumulation contribution differences between lacustrine organic-rich shales and mudstones and their significance in shale oil evaluation," *Petroleum Exploration and Development*, vol. 47, no. 6, pp. 1160–1171, 2020.

[12] Q. Lei, J. P. Latham, C. F. Tsang, J. S. Jiansheng Xiang, and P. Lang, "A new approach to upscaling fracture network models while preserving geostatistical and geomechanical characteristics," *Journal of Geophysical Research: Solid Earth*, vol. 120, no. 7, pp. 4784–4807, 2015.

[13] W. C. Fang, H. Q. Jiang, J. J. Li et al., "A numerical simulation model for multi-scale flow in tight oil reservoirs," *Petroleum Exploration & Development*, vol. 44, no. 3, pp. 446–453, 2017.

[14] G. T. Hou, X. W. Sun, and W. Ju, *Quantitative Analysis of Tight Sandstone Fractures in Kuqa Depression*, Science Press, Beijing, China, 2019.

[15] Q. Boersma, W. Athmer, M. Haege, M. Etchebes, J. Haukås, and G. Bertotti, "Natural fault and fracture network characterization for the southern ekofisk field: a case study integrating seismic attribute analysis with image log interpretation," *Journal of Structural Geology*, vol. 141, article 104197, 2020.

[16] Q. Boersma, W. Athmer, M. Etchebes, J. Haukås, and G. Bertotti, "Natural fracture prediction: a multiscale integration of seismic data, image logs and numerical forward modelling," in *81st EAGE Conference and Exhibition 2019*, pp. 3–6, London, UK, 2019.

[17] J. S. Liu, W. L. Ding, J. S. Dai, Z. H. Wu, and H. M. Yang, "Quantitative prediction of lower order faults based on the finite element method: a case study of the m35 fault block in the western hanliu fault zone in the Gaoyou sag, East China," *Tectonics*, vol. 37, no. 10, pp. 3479–3499, 2018.

[18] J. S. Liu, W. L. Ding, H. M. Yang et al., "3D geo-mechanical modeling and numerical simulation of in-situ stress fields in shale reservoirs: a case study of the Lower Cambrian Niutitang formation in the Cen'gong block, South China," *Tectonophysics*, vol. 712–713, pp. 663–683, 2017.

[19] T. H. Wilson, S. Valerie, and A. Brown, "Developing a model discrete fracture network, drilling, and enhanced oil recovery strategy in an unconventional naturally fractured reservoir using integrated field, image log, and three-dimensional seismic data," *AAPG Bulletin*, vol. 99, no. 4, pp. 735–762, 2015.

[20] D. Doolaeghe, P. Davy, J. D. Hyman, and C. Darcel, "Graph-based flow modeling approach adapted to multiscale discrete-fracture-network models," *Physical Review E*, vol. 102, no. 5, article 53312, 2020.

[21] D. Shaoqun, Z. Lianbo, D. Xiangyi et al., "An intelligent prediction method of fractures in tight carbonate reservoirs," *Petroleum Exploration and Development*, vol. 49, no. 6, pp. 1364–1376, 2022.

[22] D. Shaoqun, L. Zeng, and X. Che, "Application of artificial intelligence in fracture identification using well logs in tight reservoirs," *Earth Science*, vol. 66, 2022.

[23] M. Sahimi and M. Hashemi, "Wavelet identification of the spatial distribution of fractures," *Geophysical Research Letters*, vol. 28, no. 4, pp. 611–614, 2001.

[24] B. Tokhmechi, H. Memarian, H. A. Noubari, and B. Moshiri, "A novel approach proposed for fractured zone detection using petrophysical logs," *Journal of Geophysics and Engineering*, vol. 6, no. 4, pp. 365–373, 2009.

[25] B. Tokhmechi, H. Memarian, V. Rasouli, H. A. Noubari, and B. Moshiri, "Fracture detection from water saturation log data using a Fourier–wavelet approach," *Fourier–wavelet approach: Journal of Petroleum Science and Engineering*, vol. 69, no. 1-2, pp. 129–138, 2009.

[26] S. I. Ozkaya and S. Siyabi, "Detection of fracture corridors from dynamic data by factor analysis," in *SPE Kingdom of Saudi Arabia Annual Technical Symposium and Exhibition*, pp. 1–10, Al-Khobar, Saudi Arabia, 2008.

[27] B. Tokhmechi, H. Memarian, and M. R. Rezaee, "Estimation of the fracture density in fractured zones using petrophysical logs," *Journal of Petroleum Science Engineering*, vol. 72, no. 1–2, pp. 206–213, 2010.

[28] A. Ja'fari, A. Kadkhodaie-Ilkhchi, Y. Sharghi, and K. Ghanavati, "Fracture density estimation from petrophysical log data using the adaptive neuro-fuzzy inference system," *Journal of Geophysics and Engineering*, vol. 9, no. 1, pp. 105–114, 2012.

[29] S. Dong, L. Zeng, W. Lyu et al., "Fracture identification by semi-supervised learning using conventional logs in tight sandstones of Ordos basin, China," *Journal of Natural Gas Science and Engineering*, vol. 76, article 103131, 2020.

[30] M. Khafagy, S. Dickson-Anderson, and W. El-Dakhakhni, "A rapid, simplified, hybrid modeling approach for simulating solute transport in discrete fracture networks," *Computers and Geotechnics*, vol. 151, article 104986, 2022.

[31] J. D. Dreuzy, P. Davy, and O. Bour, "Hydraulic properties of two-dimensional random fracture networks following a power law length distribution: 2. Permeability of networks based on lognormal distribution of apertures," *Water Resources Research*, vol. 37, no. 8, pp. 2079–2095, 2001.

[32] A. Chamoli, A. R. Bansal, and V. P. Dimri, "Wavelet and rescaled range approach for the Hurst coefficient for short and long time series," *Computers & Geosciences*, vol. 33, no. 1, pp. 83–93, 2007.

[33] H. M. Almani, S. M. Hosseini, and M. Tahmasebi, "Fractional Brownian motion with two-variable Hurst exponent," *Journal of Computational and Applied Mathematics*, vol. 388, no. 776, article 113262, 2020.

[34] S. Pal, S. Dutta, T. Nasrin, and S. Chattopadhyay, "Hurst exponent approach through rescaled range analysis to study the time series of summer monsoon rainfall over Northeast India," *Theoretical and Applied Climatology*, vol. 142, no. 1-2, pp. 581–587, 2020.

[35] S. Dolan, C. Bean, and B. Riollet, "The broad-band fractal nature of heterogeneity in the upper crust from petrophysical logs," *Geophysical Journal of the Royal Astronomical Society*, vol. 132, no. 3, pp. 489–507, 1998.

[36] P. Leary, "Deep borehole log evidence for fractal distribution of fractures in crystalline rock," *Geophysical Journal International*, vol. 107, no. 3, pp. 615–627, 1991.

[37] F. Julia, W. Gale, S. E. Laubach, J. E. Olson, P. Eichhubl, and A. Fall, "Natural fractures in shale: a review and new observations," *AAPG Bulletin*, vol. 98, no. 11, pp. 2165–2216, 2014.

[38] R. Liu, Y. Jiang, B. Li, and X. Wang, "A fractal model for characterizing fluid flow in fractured rock masses based on randomly distributed rock fracture networks," *Computers and Geotechnics*, vol. 65, pp. 45–55, 2015.

[39] G. Aghli, B. Soleimani, R. Moussavi-Harami, and R. Mohammadian, "Fractured zones detection using conventional petrophysical logs by differentiation method and its correlation with image logs," *Journal of Petroleum Science and Engineering*, vol. 142, pp. 152–162, 2016.

[40] C. Y. Liu, H. G. Zhao, X. J. Gui, L. P. Yue, J. F. Zhao, and J. Q. Wang, "Space-time coordinate of the evolution and reformation and mineralization response in Ordos basin," *Acta Geological Sinica*, vol. 80, no. 5, p. 22, 2006.

[41] W. Ju, W. F. Sun, and G. T. Hou, "Insights into the tectonic fractures in the Yanchang formation interbedded sandstone-mudstone of the Ordos basin based on core data and geomechanical models," *Acta Geologica Sinica*, vol. 89, no. 6, pp. 1986–1997, 2015.

[42] W. Y. Lyu, L. B. Zeng, Z. Q. Liu, G. P. Liu, and K. W. Zu, "Fracture responses of conventional logs in tight-oil sandstones: a case study of the Upper Triassic Yanchang formation in Southwest Ordos basin, China," *AAPG Bulletin*, vol. 100, no. 9, pp. 1399–1417, 2016.

[43] W. Y. Lyu, L. B. Zeng, S. B. Zhou et al., "Natural fractures in tight-oil sandstones: a case study of the Upper Triassic Yanchang formation in the southwestern Ordos basin, China," *AAPG Bulletin*, vol. 103, no. 10, pp. 2343–2367, 2019.

[44] L. B. Zeng, W. Y. Lyu, Y. Z. Zhang, G. P. Liu, and S. Q. Dong, "The effect of multi-scale faults and fractures on oil enrichment and production in tight sandstone reservoirs: a case study in the southwestern Ordos basin, China," *Frontiers in Earth Science*, vol. 9, 2021.

[45] J. D. Gao, *Identification and Modeling of Tight Sandstone Natural Fractures in Chang 7 Section of Triassic Yanchang Formation in Jiyuan Oilfield, Ordos Basin*, Xi 'an: Northwest University, 2018.

[46] J. D. Gao, L. F. Zhou, Q. Feng, and Z. Q. Mou, "Progress in reservoir structural fracture characterization and prediction," *Geological Science and Technology Information*, vol. 37, no. 4, pp. 158–166, 2018.

[47] J. D. Gao, L. F. Zhou, and Q. Feng, "The characteristics and formation phase of structural fracture of the Jiyuan-Yuancheng area in the Ordos basin," *Journal of Geodesy and Geodynamics*, vol. 38, no. 8, pp. 811–817, 2018.

[48] E. Tóth, E. Hrabovszki, F. Schubert, and T. M. Tóth, "Discrete fracture network (DFN) modelling of a high-level radioactive waste repository host rock and the effects on its hydrogeological behaviour," *Journal of Structural Geology*, vol. 156, article 104556, 2022.

[49] T. M. Toth, "Determination of geometric parameters of fracture networks using 1d data," *Journal of Structural Geology*, vol. 32, no. 7, pp. 878–885, 2010.

[50] H. E. Hurst, "Long-term storage capacity of reservoirs," *Transactions of the American Society of Civil Engineers*, vol. 116, no. 12, pp. 776–808, 1951.

[51] M. J. Cannon, D. B. Percival, D. C. Caccia, G. M. Raymond, and J. B. Bassingthwaighte, "Evaluating scaled windowed variance methods for estimating the Hurst coefficient of time series," *Physica A Statistical Mechanics & Its Applications*, vol. 241, no. 3-4, pp. 606–626, 1997.

[52] J. Pang and C. P. North, "Fractals and their applicability in geological wireline log analysis," *Journal of Petroleum Geology*, vol. 19, no. 3, pp. 339–350, 1996.

[53] Z. K. Xiao, W. L. Ding, J. S. Liu et al., "A fracture identification method for low-permeability sandstone based on R/S analysis and the finite difference method: a case study from the Chang 6 reservoir in Huaqing oilfield, Ordos basin," *Journal of Petroleum Science and Engineering*, vol. 174, pp. 1169–1178, 2019.

[54] M. Li, "Fractal time series—a tutorial review," *Mathematical Problems in Engineering*, vol. 2010, Article ID 157264, 26 pages, 2010.

[55] J. G. Berryman and V. Grechka, "Random polycrystals of grains containing cracks: model of quasistatic elastic behavior for fractured systems," *Journal of Applied Physics*, vol. 100, no. 11, article 113527, 2006.

[56] S. R. Pride and J. G. Berryman, "Linear dynamics of double-porosity dual-permeability materials. II. Fluid transport equations," *Physical Review E*, vol. 68, no. 3, article 036604, 2003.

[57] S. Q. Chen, L. B. Zeng, P. Huang, S. H. Sun, W. L. Zhang, and X. Y. Li, "The application study on the multi-scales integrated prediction method to fractured reservoir description," *Applied Geophysics*, vol. 13, no. 1, pp. 80–92, 2016.

[58] C. Cranganu and E. Bautu, "Using gene expression programming to estimate sonic log distributions based on the natural gamma ray and deep resistivity logs: a case study from the Anadarko basin, Oklahoma," *Journal of Petroleum Science & Engineering*, vol. 70, no. 3-4, pp. 243–255, 2010.

[59] X. L. Zhang, Q. Feng, P. Sun, and W. Li, "Characteristics of high-gamma-ray sandstone reservoirs for Yanchang formation

in Ordos basin," *Chinese Journal of Geophysics*, vol. 53, no. 1, pp. 154–163, 2010.

[60] A. Yaghoubi, "Hydraulic fracturing modeling using a discrete fracture network in the Barnett Shale," *International Journal of Rock Mechanics and Mining Sciences*, vol. 119, pp. 98–108, 2019.

[61] N. Gunnarsson, *3D Modeling in Petrel of Geological CO_2 Storage Site*, Department of Earth Sciences, 2011.

[62] S. H. Zhang, *Identification of Low Contrast Oil Layers in Chang 8 and Chang 9 Oil Layers of Yanchang Formation in Mahuangshan-Gufengzhuang Area, Western Ordos Bain*, Northwest University, Xi'an, China, 2021.